The Structure of Photosystem II and the Mechanism of Water Oxidation in Photosynthesis

Jian-Ren Shen

Photosynthesis Research Center, Graduate School of Natural Science and Technology, Okayama University, Okayama 700-8530, Japan; email: shen@cc.okayama-u.ac.jp

Key Laboratory of Photobiology, Institute of Botany, Chinese Academy of Sciences, Beijing 100093, China

Annu. Rev. Plant Biol. 2015. 66:23–48

First published online as a Review in Advance on February 26, 2015

The *Annual Review of Plant Biology* is online at plant.annualreviews.org

This article's doi: 10.1146/annurev-arplant-050312-120129

Keywords

crystal structure, membrane proteins, oxygen evolution, photosynthesis, photosystem II, S state, water splitting

Abstract

Oxygenic photosynthesis forms the basis of aerobic life on earth by converting light energy into biologically useful chemical energy and by splitting water to generate molecular oxygen. The water-splitting and oxygen-evolving reaction is catalyzed by photosystem II (PSII), a huge, multisubunit membrane-protein complex located in the thylakoid membranes of organisms ranging from cyanobacteria to higher plants. The structure of PSII has been analyzed at 1.9-Å resolution by X-ray crystallography, revealing a clear picture of the Mn_4CaO_5 cluster, the catalytic center for water oxidation. This article provides an overview of the overall structure of PSII followed by detailed descriptions of the specific structure of the Mn_4CaO_5 cluster and its surrounding protein environment. Based on the geometric organization of the Mn_4CaO_5 cluster revealed by the crystallographic analysis, in combination with the results of a vast number of experimental studies involving spectroscopic and other techniques as well as various theoretical studies, the article also discusses possible mechanisms for water splitting that are currently under consideration.

Contents

INTRODUCTION

Oxygenic photosynthesis provides us with food and oxygen, both of which are indispensable for maintaining aerobic life on earth. The first reaction in photosynthesis occurs in photosystem II (PSII), which catalyzes a series of light-induced electron-transfer reactions that lead to the splitting of water molecules. These reactions result in the conversion of light energy into biologically useful chemical energy and the evolution of molecular oxygen. Thus, photosynthetic water splitting is one of the most important biochemical reactions on earth (3, 4).

PSII is a large membrane-protein complex located in the thylakoid membranes of organisms ranging from cyanobacteria to higher plants. In cyanobacteria, it contains 20 subunits, of which 17 are transmembrane subunits and 3 are membrane-peripheral, extrinsic subunits, with a total molecular mass of 350 kDa (108, 131). PSII in cyanobacteria typically exists in a dimeric form (54, 59, 111) and thus has a total molecular mass of 700 kDa. Among the transmembrane subunits, D1 and D2 (the gene products of *psbA* and *psbD*, respectively) have five transmembrane helices each and constitute the reaction center core of PSII, with which all of the cofactors participating in the electron-transfer and water-splitting reactions are associated (23, 31, 46, 69, 108, 127, 131, 149). Surrounding the D1 and D2 subunits are the CP47 and CP43 subunits (the gene products of *psbB* and *psbC*, respectively; CP stands for chlorophyll protein), which have six transmembrane helices each and bind a number of chlorophyll (Chl) molecules to serve an intrinsic (inner) light-harvesting function. In addition to these 4 large subunits, there are 13 low-molecular-weight transmembrane subunits: PsbE, PsbF, PsbH, PsbI, PsbJ, PsbK, PsbL, PsbM, PsbT, PsbX, PsbY, PsbZ, and Psb30. These subunits have molecular masses of less than 10 kDa and one transmembrane helix each except for PsbZ, which has two transmembrane helices (23, 31, 108, 127, 131).

PSII: photosystem II
Chl: chlorophyll

The 3 membrane-peripheral, extrinsic proteins are associated with the lumenal side of PSII and are necessary to maintain the water-splitting reaction. In cyanobacteria, these subunits are

PsbO (33 kDa), PsbU (12 kDa), and PsbV (cytochrome c_{550}, 17 kDa) (22, 109, 110); in green algae and higher plants, PsbU and PsbV are replaced with PsbQ and PsbP (9, 22, 40, 101).

The cluster of reaction center Chls in PSII is referred to as P680; it comprises four Chls bound to the D1 and D2 subunits (21, 95, 97, 131). Upon absorption of light energy, one of the Chls becomes excited and donates one electron to the initial electron acceptor pheophytin, which subsequently transfers the electron to the primary and secondary plastoquinone acceptors, referred to as Q_A and Q_B, respectively. The oxidized P680 is reduced by a nearby tyrosine residue, Tyr161 of the D1 subunit designated Y_Z (5, 20, 120, 131), which in turn oxidizes a Mn_4CaO_5 cluster, which is the catalytic center for water splitting. Once four electrons have been abstracted from the Mn_4CaO_5 cluster, two water molecules are split into four protons and one oxygen molecule. Thus, the water-splitting reaction is a four-electron reaction that proceeds through the S_i-state cycle, where $i = 0$–4 (the so-called Kok cycle) (43, 44, 56). S_0 is the most reduced state, whereas S_1 is dark stable, and oxygen is produced during the S_3–(S_4)–S_0 transition. S_0 is oxidized gradually in the dark by Y_D^+, an analog of Y_Z bound to the D2 subunit (D2-Tyr160) (119, 120, 128).

P680: the reaction center chlorophylls of PSII

Q_A and Q_B: the primary and secondary plastoquinone acceptors, respectively, in PSII

Y_Z: the primary electron donor to the reaction center in PSII

To understand the water-splitting mechanism, it is essential to elucidate the structure of the Mn_4CaO_5 cluster and its surrounding protein environment. For this purpose, the PSII dimer complex from thermophilic cyanobacteria has been successfully crystallized, and its structure has been solved at resolutions that have gradually increased to 1.9 Å over the past 15 years (23, 31, 46, 69, 127, 149). This atomic-resolution structure has revealed the detailed organization of protein subunits, electron-transfer cofactors, and in particular the structure of the Mn_4CaO_5 cluster as well as a vast number of water molecules associated with the protein matrix. In the following, I first briefly review the history of the crystallization and structural analysis of PSII, then describe the overall structure of PSII and the detailed organization of the Mn_4CaO_5 cluster. Based on the structural analysis as well as other spectroscopic and theoretical studies, I then discuss the water-splitting mechanisms currently under consideration.

CRYSTALLIZATION AND CRYSTAL STRUCTURE ANALYSIS OF PHOTOSYSTEM II

The first crystals of PSII dimers were obtained by Zouni et al. (148) from the thermophilic cyanobacterium *Thermosynechococcus elongatus*, and its structure was reported at a resolution of 3.8 Å in 2001 (149). The use of the thermophilic cyanobacterium was important for the success of crystallization because the PSII core dimer from this bacterium is highly stable and active (110, 121). In this structure, the positions of the major PSII subunits were assigned in a Cα model together with the position of the Mn_4Ca cluster that catalyzes the water-splitting reaction (at the time, this cluster was generally referred to as the Mn_4Ca cluster because its exact composition was not known). The side-chain structures of the amino acids and the positions of some small subunits were not given owing to the limited resolution. Subsequently, Kamiya & Shen (46) reported a 3.7-Å structure of the PSII dimer from a closely related thermophilic cyanobacterium, *Thermosynechococcus vulcanus*, in which a few more subunits were assigned together with the side chains of some residues. However, the structure of the Mn_4Ca cluster remained unclear because each of the metal atoms and the presumed oxo-bridges connecting the metal atoms were not separated in the electron density map, making the electron density of the metal cluster like that of a ball packed with all five of the metal ions and possible oxo-bridges.

The resolution of the PSII structure increased gradually to 3.5 Å (23), 3.0 Å (69), and 2.9 Å (31), which continuously improved the structure of the whole complex in terms of the side-chain orientations of amino acid residues and a number of cofactors, such as Chls, carotenoids, lipids, and a bicarbonate ion. The presence of Ca^{2+} as an integral part of the water-oxidizing

catalyst was demonstrated by several biochemical and biophysical studies, including those using electron paramagnetic resonance (EPR) and extended X-ray absorption fine structure (EXAFS) measurements (132, 145); the global position of this ion in the Mn_4Ca cluster was first identified in the 3.5-Å structure from anomalous scattering at a wavelength near the Ca^{2+} absorption edge (23) and was subsequently confirmed by the higher-resolution structures (31, 69). The 3.5-Å structure also suggested a cuboidal model for the Mn_4Ca cluster; however, its detailed structure as well as the exact ligand pattern, the positions of water molecules, etc., remained obscure because the electron densities for the atoms were still not separated. This meant that the positions of the individual atoms could not be clearly determined from the experimentally obtained electron densities, and the structural models had to incorporate constraints from previous results, mainly from EXAFS studies.

EPR: electron paramagnetic resonance

EXAFS: extended X-ray absorption fine structure

H-bond: hydrogen bond

In 2011, Umena et al. (127) reported the atomic structure of the PSII dimer complex at a resolution of 1.9 Å. At this resolution, the electron densities of the individual atoms in the Mn_4Ca cluster were clearly separated, allowing the structure of the metal cluster to be determined unambiguously. In addition, the structure revealed the coordination environment of the metal cluster in much more detail than the previously obtained structure, and the positions of the oxo-bridges and terminal water ligands were identified for the first time. This atomic-resolution structure also revealed the presence of a huge number of water molecules associated with various residues in the PSII dimer, some of which form extended hydrogen-bond (H-bond) networks that may be important for the export of protons from the site of water splitting or the inlet of substrate water molecules into the reaction site (52, 127).

THE OVERALL STRUCTURE OF THE PHOTOSYSTEM II DIMER

Figure 1 shows the overall structure of the PSII dimer analyzed at 1.9-Å resolution; this structure contains 19 subunits per monomer, of which 16 are transmembrane subunits and 3 are membrane-peripheral subunits required for oxygen evolution. As mentioned above, D1 and D2 form the reaction center core complex of PSII, to which most of the electron-transfer cofactors are bound. CP47 and CP43 are located in the two sides of the D1/D2 core and bind 16 and 13 Chls, respectively, which function as light-harvesting antennae to transfer the light energy to the reaction center Chls (70, 75, 107, 108).

In addition to these large transmembrane subunits, the structure included 12 small subunits. As mentioned above, these subunits each have one transmembrane helix with the exception of PsbZ, which has two. These give rise to a total of 35 transmembrane helices for a PSII monomer. PsbY, one of the low-molecular-mass subunits with a single transmembrane helix located in the

Figure 1

The overall structure of the photosystem II (PSII) dimer. (*a*) The structure of a PSII dimer analyzed at 1.9-Å resolution, viewed from a direction perpendicular to the membrane normal. The vertical line in the middle represents the noncrystallographic twofold axis dividing the two monomers, and the two red circles indicate the regions where the water-splitting catalytic center (the Mn_4CaO_5 cluster) binds. The major PSII subunits are also indicated. (*b*) The distribution of water molecules in the PSII dimer. The proteins are omitted, and the chlorophylls (*green*), pheophytins (*cyan*), β-carotenes (*orange*), Mn_4CaO_5 cluster (*purple and red balls*), heme of cytochrome c_{550} (*red*), and nonheme iron (*pink*) are indicated in the left-hand monomer, together with all of the water molecules (*blue*). (*c*) The arrangement of transmembrane helices, chlorophylls, and other cofactors in the PSII dimer in a top view from the stromal side. The dashed line in the middle divides the two monomers, and the protein subunits are labeled in one of the monomers. The circled regions indicate D1 and D2 (*blue dashed circle*), CP47 (*cyan dashed circle*), and CP43 (*pink dashed circle*). In addition to the chlorophylls shown in the left-hand monomer (*green*), other cofactors are shown in both monomers, including β-carotenes (*yellow*), plastoquinones (*blue*), and lipids and detergents (*magenta*, *purple*, and *pink*).

peripheral region close to PsbE and PsbF (the α and β subunits of cytochrome b_{559}), was not present in the crystal structure but was present in some early low-resolution structures (46, 50, 69), indicating that it is weakly associated with the PSII core and was lost during the crystallization process.

The three peripheral, hydrophilic subunits—PsbO, PsbU, and PsbV—are located in the lumenal side of the thylakoid membrane. Together with the extrinsic loops of D1, D2, CP43, and CP47 that protrude into the lumenal side, these subunits form a cap for the site of oxygen evolution (the Mn_4CaO_5 cluster), shielding it from the lumenal bulk solution. The three extrinsic proteins are

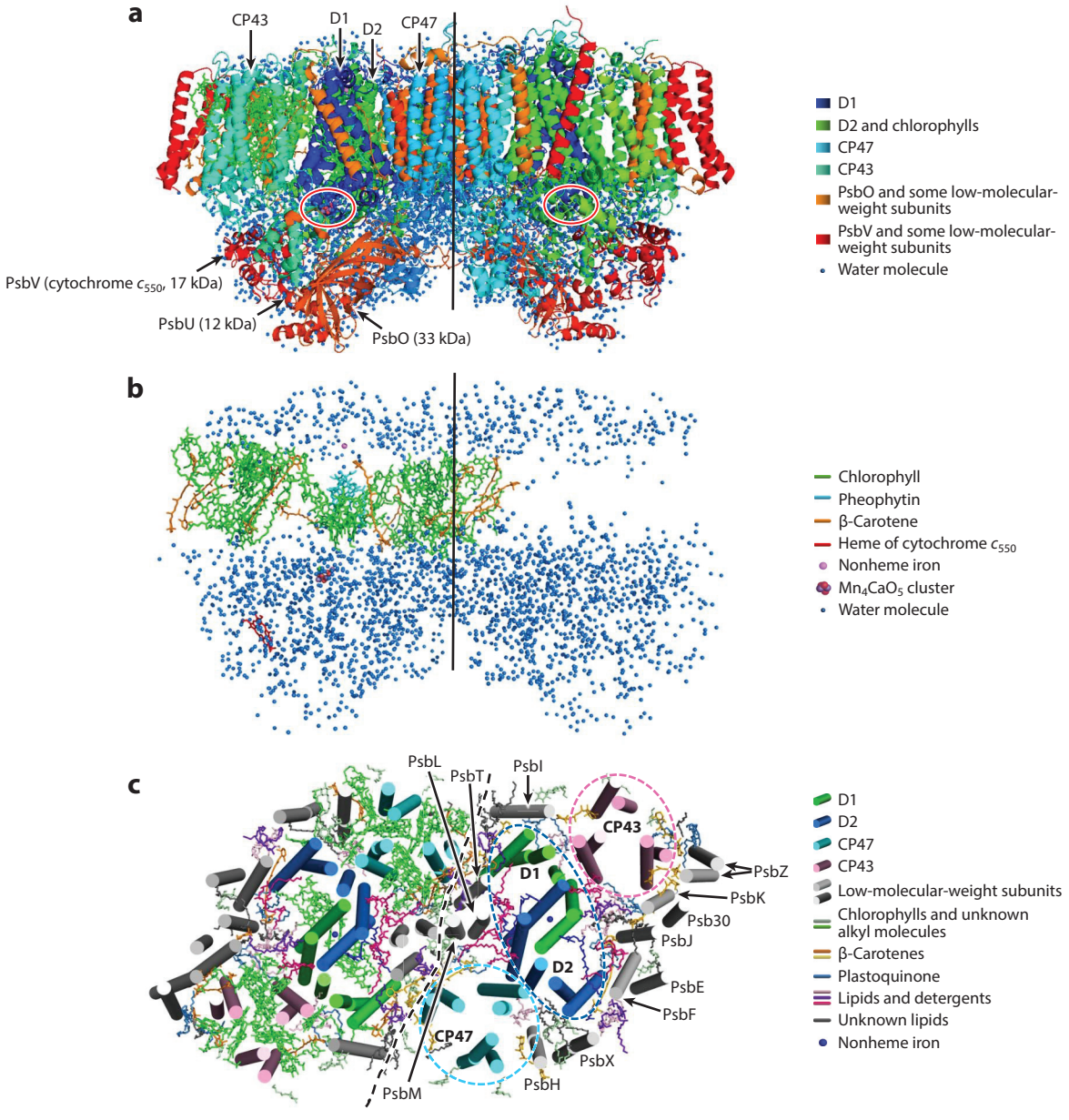

important for maintaining the activity and stability of the oxygen-evolving complex (22, 101, 110, 112). In addition to the protein subunits, PSII monomers comprise 35 Chls, 2 pheophytins, 11 β-carotenes, 2 plastoquinones, 1 bicarbonate ion, 1 *b*-type and 1 *c*-type cytochrome, 1 nonheme iron, more than 20 lipid molecules, at least 2 chlorides, 1 Mn_4CaO_5 cluster, and other components (127).

One of the most significant features of the high-resolution PSII structure was the presence of a huge number of water molecules: In total, nearly 2,800 were found in a PSII dimer (127). These water molecules were distributed in two layers, one in the surface of the cytoplasmic (stromal) side of the thylakoid membrane and the other in the surface of the lumenal side (107, 127) (**Figure 1*b***). Very few were found in the transmembrane region. These distributions demonstrate a typical feature of a membrane-protein complex. The few water molecules present in the transmembrane region serve as ligands or H-bonding partners of Chls that are not ligated by an amino acid residue. Typically, the Mg ion of the chlorin ring of Chls is ligated by an amino acid residue, in most cases a His residue. Of the 35 Chls in a PSII monomer, however, 7 do not have an amino acid residue as a ligand for their Mg ion; instead, this ion is ligated by a water molecule (127). For such Chls, there are usually two additional water molecules in the vicinity of the chlorin ring that form H-bonds to the carbonyl groups of the chlorin ring as well as the direct water ligand; these water molecules are probably necessary to stabilize the chlorin ring not directly ligated to an amino acid residue.

THE STRUCTURE OF THE Mn_4CaO_5 CLUSTER

The Crystal Structure of the Mn_4CaO_5 Cluster

The Mn_4CaO_5 cluster is bound in a pocket formed by residues of D1 and CP43 in the lumenal surface of the thylakoid membrane (circled regions in **Figure 1*a***). Because the interatomic distances within the cluster are in the range of 1.7–2.6 Å, it was not possible to separate each of the atoms in the structures at up to 2.9-Å resolution (23, 31, 46, 69, 149). In particular, the electron densities of oxygen atoms are much weaker than those of Mn and Ca^{2+} ions, and thus their assignments were highly ambiguous compared with those of the metal ions. In the 1.9-Å-resolution PSII structure (127), the electron densities for each of the metal ions and the oxo-bridged oxygen atoms were clearly separated, allowing the unambiguous assignment of each atom (**Figure 2*a***). As a result, the catalytic center for water oxidation was found to contain five oxygen atoms in addition to four Mn ions and one Ca^{2+} ion, forming a Mn_4CaO_5 cluster (**Figure 2*b***). Because Mn (with a valence of III or IV) has three or four more electrons than Ca^{2+} (with a valence of II), the electron density of the Ca^{2+} ion is slightly lower than that of the Mn ions (**Figure 2*a***). This also demonstrates the high quality of the electron density obtained at atomic resolution. The core of the cluster is a distorted cubane made up of three Mn ions (Mn1–Mn3), four oxygen atoms (O1–O3 and O5), and one Ca^{2+} ion. The fourth Mn ion (Mn4) is located outside of the cubane and connected to the cubane core by two μ-oxo-bridges via O4 and O5. The shape of the whole cluster resembles that of a distorted chair, with the cubane serving as the chair base and the outside Mn (Mn4) serving as the back of the chair (127) (**Figure 2*c***).

The distorted shape represents one of the most significant features of the Mn_4CaO_5 cluster structure: the unstable (or flexible) nature of the metal complex, which enables the cluster to easily undergo structural rearrangements during the S-state cycle. Such rearrangements would be expected to occur in an efficient catalyst for water splitting and have been suggested by studies based on a variety of spectroscopic techniques, including EPR and electron-nuclear double resonance (ENDOR) (10, 32, 60, 61, 87), EXAFS (16, 17, 28, 33, 92, 105, 139, 141), and Fourier transform

ENDOR: electron-nuclear double resonance

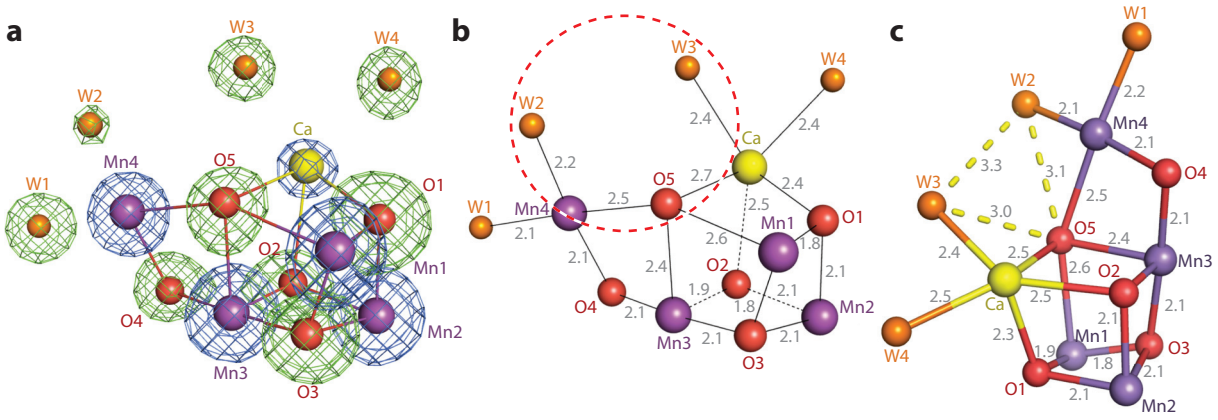

Figure 2

The structure of the Mn_4CaO_5 cluster. (*a*) Individual atoms of the Mn_4CaO_5 cluster, superimposed with the $2F_o$–F_c map (*blue*), contoured at 5 σ for Mn and Ca atoms, and with the omit map (*green*), contoured at 7σ for oxygen atoms and water molecules. (*b*) Bond distances (in angstroms) between metal ions and oxo-bridges or water molecules within the Mn_4CaO_5 cluster. The area circled with the red dashed line indicates a possible reaction region. (*c*) The distorted chair form of the Mn_4CaO_5 cluster. The structure of the cluster is rotated relative to that shown in panel *b* to show the shape more clearly. The yellow dashed lines indicate hydrogen bonds.

infrared spectroscopy (FTIR) (19, 82–84). A symmetric, rigid structure, by contrast, would make it difficult for the Mn_4CaO_5 cluster to undergo the structural changes needed for its catalytic activity. Thus, nature has developed a highly efficient water-splitting catalyst over a long period of evolution by incorporating a flexible structure into a highly complex protein environment—a prerequisite that must also be met if we are to develop an efficient artificial catalyst for water splitting.

The distortion in the structure of the Mn_4CaO_5 cluster is caused mainly by two factors. One is the differences in the Mn–O distances. Among the five oxygen atoms, O1–O4 have bond distances to their nearby Mn ions in the range of 1.8–2.2 Å, similar to the distances typically found in Mn oxide compounds containing Mn(III) or Mn(IV) (47, 48, 76, 99, 126, 141, 142). However, the distances between O5 and its nearby Mn ions in the crystal structure are much longer: 2.4 Å, 2.5 Å, and 2.6 Å for O5–Mn3, O5–Mn4, and O5–Mn1, respectively. These distances, in particular the O5–Mn4 and O5–Mn1 distances, are much longer than those expected for normal Mn oxides, suggesting a weak binding of the O5 atom to the nearby Mn ions (see below for a more detailed discussion).

The other factor contributing to the distortion in the structure of the Mn_4CaO_5 cluster is the differences in the typical Mn–O and Ca–O distances. As described above, the typical Mn–O distances are in the range of 1.8–2.2 Å, whereas the typical Ca–O distances are in the range of 2.4–2.6 Å owing to the lower positive charge of the Ca^{2+} ion compared with that of the Mn ions. The incorporation of the single Ca^{2+} ion in the metal cluster may therefore have contributed to the distorted shape of the structure, which may be important for the flexibility or catalytic activity of the catalytic core.

In addition to the oxo-bridged oxygen atoms, four water molecules are associated with the Mn_4CaO_5 cluster as terminal ligands (127). These water ligands are designated W1–W4; two of them (W1 and W2) are associated with Mn4, and the other two (W3 and W4) are associated with the Ca^{2+} ion (**Figure 2**). Interestingly, no other direct water ligands have been found to associate with the remaining three Mn ions, indicating that the region formed by Mn4, Ca^{2+}, and the four water molecules is highly hydrophilic and may play an important role in water splitting. Of

FTIR: Fourier transform infrared spectroscopy

these four water molecules, W2 (bound to Mn4) and W3 (bound to Ca^{2+}) are within H-bonding distances of O5. Furthermore, W2 and W3 are also within H-bond distance of each other. Thus, the area formed by W2, W3, and O5 may constitute the site of O-O bond formation during the water-splitting reaction (see below for further discussion).

QM/MM: quantum mechanics/molecular mechanics

The distances from the two water ligands to Mn4 are in the range of 2.1–2.2 Å, whereas those from W3 and W4 to Ca^{2+} are 2.4 Å. The slightly shorter distances between the water ligands and Mn4 reflect a higher valence of Mn4 compared with Ca^{2+} and thus a slightly stronger binding of the water ligands to Mn4 than to Ca^{2+}.

Mn–Mn and Mn–O Distances in the Mn_4CaO_5 Cluster: Comparisons Between the Experimental Results and Theoretical Calculations

The shortest distances between Mn ion pairs in the 1.9-Å-resolution crystal structure are 2.8 Å for Mn1–Mn2, 2.9 Å for Mn2–Mn3, and 3.0 Å for Mn3–Mn4. These distances are in general agreement with the results of EXAFS experiments, which suggested that there were two short Mn–Mn distances and one long Mn–Mn distance (16, 18, 30, 98, 139–142). However, the short and long distances suggested by these experiments were 2.7 Å and 2.8 Å, respectively, which are 0.1–0.2 Å shorter than the distances obtained from the crystal structural analysis (17, 18, 30, 33, 91, 98, 139–142, 146).

These differences between the crystal structure and the EXAFS results may fall within the experimental error, as the results of crystal structure analysis at 1.9-Å resolution bear an average error of 0.16 Å for the interatomic distances (127). Therefore, theoretical calculations using the coordinates of the crystal structure have been performed to examine the Mn–Mn as well as Mn–O distances. Extensive quantum mechanics/molecular mechanics (QM/MM) calculations using the coordinates of the crystal structure have resulted in model structures for the Mn_4CaO_5 cluster where the shortest Mn–Mn distances resemble those of the EXAFS results but are slightly shorter (0.1–0.2 Å) than those of the crystal structure (2, 25, 30, 42, 49, 63, 64, 71, 89, 116, 117, 133–137). This has been taken as evidence that the crystal structure is in a reduced state, probably a mixture of S_0 and super-reduced states from S_{-1} to S_{-3}, rather than the S_1 state presumed in the X-ray structural analysis, which may have resulted from radiation damage [albeit much reduced compared with previous studies (23, 31, 46, 69, 149)] caused by the X-ray illumination used to collect the diffraction data (29, 138).

Although the possibility of radiation damage cannot be excluded at present, there is another potential source of the differences that needs to be considered. Because the H atom cannot be assigned in the X-ray structure analysis at 1.9-Å resolution, the four terminal water ligands have been assumed to be H_2O, and the five oxo-bridged oxygen atoms have been assigned as O^{2-}. It is possible that the protonation states of some of the water molecules and/or oxo-bridges are different from those assumed in the crystal structure, and the exact combination of the protonation states is not known. A combination of the protonation states different from those of the real structure may affect the results of theoretical calculations (14, 30, 42, 49, 89, 99, 100, 104, 133–137).

More profound differences between the crystal structure and the theoretical calculations were found in the Mn1–O5 and Mn4–O5 distances. As described above, the O5 atom is located almost midway between Mn1 and Mn4 (center structure), resulting in unusually long distances to both Mn1 and Mn4 that have never been obtained in theoretical calculations if the O5 atom is in a deprotonated state (O^{2-}). Assuming that O5 is in this form, theoretical calculations yielded a result showing that the Mn4–O5 distance is in the range of 1.8–2.1 Å, whereas the Mn1–O5 distance is in the range of 3.0–3.3 Å (2, 25, 30, 42, 71, 89, 116, 117, 133–137). This results in an open-cubane structure, with no bond between O5 and Mn1 (right-side-open structure; **Figure 3*a***). In this case,

Mn4 is 6-coordinated whereas Mn1 is 5-coordinated in the S_1 state. This is remarkably different from the crystal structure, which suggested a quasi-5-coordinated structure for both Mn4 and Mn1 in the S_1 state. The nearly central position of the O5 atom between Mn1 and Mn4 observed in the current crystal structure strongly suggests that the O5 atom has a labile (flexible) nature (42, 49, 104, 113, 133–137), enabling it to move easily toward Mn1 or Mn4 following slight changes in the environment.

In an attempt to explain the unusually long O5–Mn4 and O5–Mn1 distances observed experimentally, QM/MM calculations have been performed assuming that O5 is in a protonated state, namely, an OH^- form, the result of which showed that the O5–Mn4 and O5–Mn1 distances are rather comparable to those observed in the crystal structure (42, 104, 133–137). This suggests that O5 may be in a protonated state. Alternatively, the theoretical calculations performed so far may not have incorporated the protein environment surrounding the Mn_4CaO_5 cluster in an area large enough to account for the precise structure of the cluster. It should be pointed out that distances below 2.0 Å for O5–Mn4 and above 3.0 Å for O5–Mn1 are unlikely given the current resolution of the crystal structure, underscoring the need to carefully examine the protonation states in the Mn_4CaO_5 cluster on which the theoretical calculations are based.

Interestingly, theoretical calculations based on the crystal structure yielded an S_2 state involving both right-side-open (R-type) and left-side-open (L-type) structures where the O5 is coordinated to either Mn4 or Mn1 (42, 86) (**Figure 3**), and the two structural types are easily interconvertible, consistent with the labile nature of O5 in the S_1 state suggested by the crystal structure analysis. The R-type structure has been suggested to correspond with the S_2 state that gives rise to the well-known low-spin ($S = 1/2$) multiline EPR signal, whereas the L-type structure corresponds to the S_2 state that gives rise to the high-spin ($S = 1/2$), $g = 4.0$ EPR signal (86). Under normal conditions, the multiline EPR signal dominates in the S_2 state, and therefore the R-type structure should also be the dominant one.

During the S_1–S_2 transition, no proton is released and no significant structural changes have been observed (28, 45, 123, 142). Therefore, the S_1 state may also adopt two types of structures—namely, R- and L-type structures, as suggested from theoretical calculations—although which one dominates in the S_1 state is not known. As mentioned above, this is different from what was observed in the 1.9-Å crystal structure; the causes for this discrepancy may include radiation

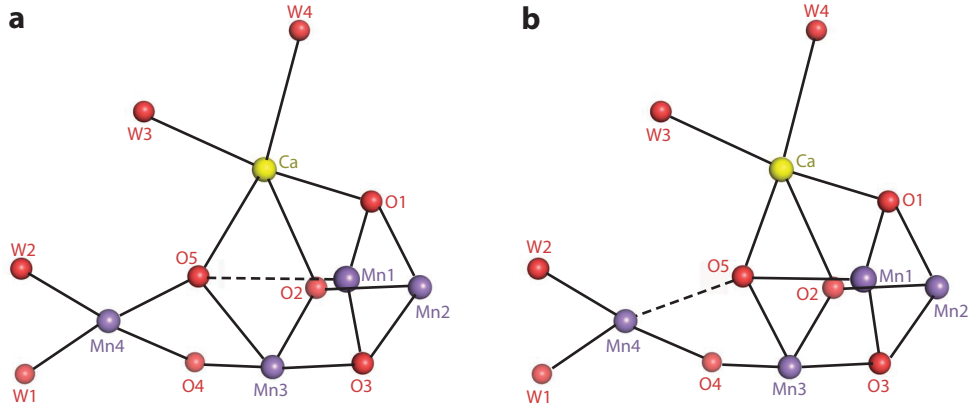

Figure 3

The (*a*) right-side-open and (*b*) left-side-open structures of the Mn_4CaO_5 cluster. The dashed lines indicate the breakage of bonds.

damage, different protonation states assumed for the calculations, or the effects of protein environments surrounding the metal cluster, which may be difficult to evaluate explicitly in the current QM/MM calculations. It should be pointed out that the relative positions of Mn4, O5, and Mn1 likely change during the S_1–S_2 transition, because during this transition an electron is removed from the Mn_4CaO_5 cluster. Multifrequency electron-spin-echo envelope-modulation (ESEEM) spectroscopic measurements (106, 143, 144) have implied that the Mn1 ion is in a III oxidation state in S_2, and therefore it must also be in the III state in S_1. Based on the high-oxidation scenario, the Mn1–Mn4 ions have oxidation states of III, III, IV, and IV, respectively, in S_1 (10, 33, 60, 61, 87, 142–144; for a low-oxidation scenario, see 26, 27, 57, 85, 89). If we assume that the Mn4 ion is also in a III state in S_1, then both Mn1 and Mn4 would have a large Jahn-Teller axis, leading to longer bond distances to O5, as were observed in the crystal structure. Upon transition from S_1 to S_2, the electron must be removed from Mn4, putting that ion in the IV state while leaving Mn1 in the III state. This would force O5 to move toward Mn4, resulting in the R-type structure. Alternatively, theoretical calculations have shown that the R- and L-type structures have very small differences in energy level, suggesting that they are easily interconvertible (42, 86). Thus, in some fractions of the center, Mn1 may be oxidized instead of Mn4, resulting in the L-type structure in S_2.

As discussed above, the unusual position of O5 observed in the crystal structure suggested that it is in a protonated state (OH^-) in S_1, which would mean that it must also have a proton on it in S_2, because no proton is released during the S_1–S_2 transition (45, 123). This is in contrast to the magnetic measurements and theoretical calculations showing that no protonated oxo-bridges are detectable in the S_2 state (2, 14, 15, 68, 93, 100). A plausible explanation for this discrepancy is that an intramolecular proton transfer occurs during this transition, so that the proton on O5 is transferred to somewhere within the oxygen-evolving complex or residues nearby this complex, for example, W2 or D1-Asp61 (42, 104, 133–137). In any case, the unusual position of O5 is consistent with the above discussions that the area surrounding O5 may form the reaction site for water splitting and O-O bond formation.

The Ligand Environment of the Mn_4CaO_5 Cluster

The Mn_4CaO_5 cluster is coordinated by seven amino acids, of which six are carboxylate residues and one is a His residue (127) (**Figure 4*a***). The six carboxylate residues are D1-Asp170, D1-Glu189, D1-Glu333, D1-Asp342, D1-Ala344, and CP43-Glu354; all of these are bidentate ligands with the exception of D1-Glu189, which is a monodentate ligand to Mn1. D1-Ala344 is the C-terminal residue of the D1 subunit, and D1-His332, D1-Glu333, and D1-Asp342 are located in the C-terminal region of the D1 subunit, indicating that the C-terminal domain of the D1 subunit is heavily involved in maintaining the structure of the Mn_4CaO_5 cluster. The His residue is D1-His332, which is ligated to Mn1. These ligands, together with the oxo-bridges and terminal water ligands, constitute a saturated ligand environment for the Mn_4CaO_5 cluster, in which all four Mn ions are 6-coordinated (see above discussions of Mn4 and Mn1), whereas the Ca^{2+} ion is 7-coordinated.

Perhaps one of the most important factors that makes the Mn_4CaO_5 cluster unique is the coordination pattern of the μ-oxo-bridged oxygen atoms. In addition to their direct coordination to the nearby metal ions, all five oxo-bridged oxygen atoms are H-bonded to either amino acid residues or water molecules (**Figure 4*b***). Among the five oxygen atoms, O1–O3 are each bonded to three metal ions and have additional H-bonds. O1 is H-bonded to a water molecule [W923; the numbering of water molecules is based on Protein Data Bank (PDB) ID 3ARC, with the exceptions of W1–W4], D1-Glu189/OE1 and OE2, and the two carboxylate oxygen atoms of D1-Ala344;

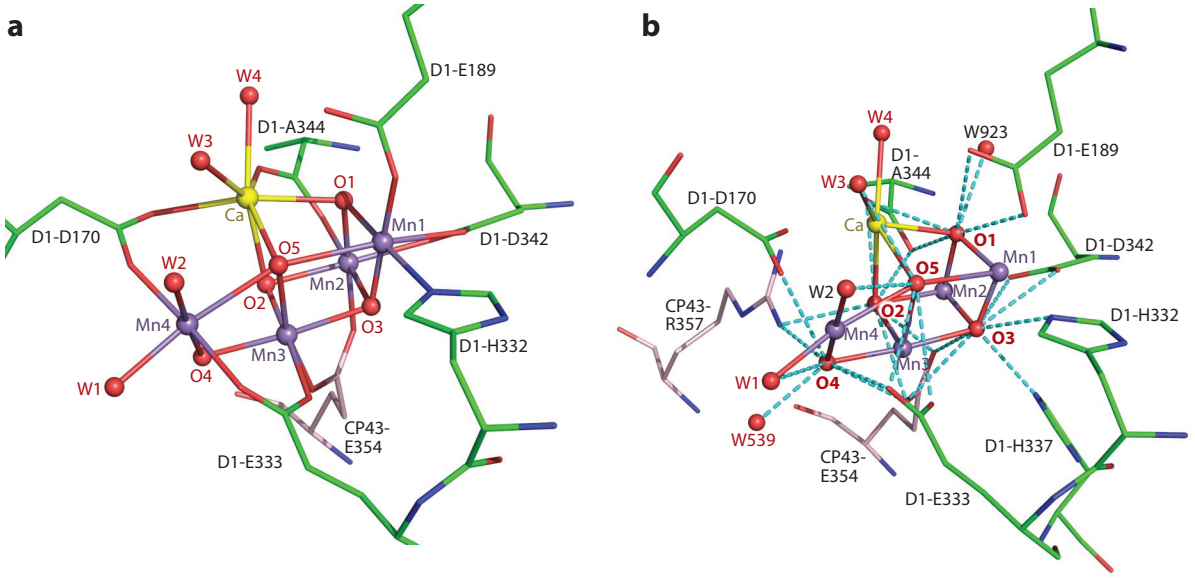

Figure 4

The ligand environment of the Mn_4CaO_5 cluster. (*a*) Direct (first coordinate) ligands to the Mn_4CaO_5 cluster, showing that each Mn ion has six ligands, whereas the Ca^{2+} ion has seven ligands. (*b*) Hydrogen bonds (*cyan dashed lines*) to the five oxo-bridged oxygen atoms (*bold*). For clarity, the metal cluster is rotated relative to the view in panel *a*. In both panels, D1 subunits are shown in green, CP43 subunits are shown in pink, Mn ions are shown in purple, Ca ions are shown in yellow, and oxygen atoms are shown in red.

O2 is H-bonded to CP43-Arg357/NH2, CP43-Glu354/OE1 and OE2, and the two carboxylate oxygen atoms of D1-Ala344; and O3 is H-bonded to D1-His332/NE2, D1-His337/NE2, D1-Asp342/OD1 and OD2, and CP43-Glu354/OE1 and OE2. These H-bonds give these three oxygen atoms a tetrahedral structure, fulfilling the octet rule for the coordination of oxygen dianions (80, 104) except for O3, which has an additional H-bond. Because the four residues H-bonded to O3 are also H-bonded to other oxygen atoms or coordinated to the metal ions, it is possible that one of these residues within H-bond distance of O3 is not actually H-bonded to O3, in which case O3 would still fulfill the octet rule. The O4 atom linking the dangling Mn (Mn4) to the cubane is oxo-bridged to two Mn ions (Mn3 and Mn4) and has six additional H-bonds with W1, an additional water molecule (W539), D1-Asp170, D1-Glu333, CP43-Glu354, and CP43-Arg357. Thus, O4 also has a tetrahedral structure. Compared with these four oxygen atoms, O5 is bridged to four metal ions (Mn1, Mn3, Mn4, and Ca^{2+}) and also H-bonded to four other species, W2, W3, and D1-Glu333/OE1 and OE2. Furthermore, O5 is also close to D1-Glu189/OE2 (3.37 Å). This may make the O5 atom unique among the five oxo-bridged atoms, making it a good candidate for the water oxidation substrate, which is consistent with the discussion above based on the unusual position and bond distances of O5 to the nearby metal ions.

An important role of the H-bonds to the oxo-bridges provided by two positively charged residues (CP43-Arg357 and D1-His337) may be to partially compensate for the negative charges of the oxygen dianions within the Mn_4CaO_5 cluster, thereby weakening the bond between oxygen dianions and Mn(III), Mn(IV), or the Ca^{2+} ion. This may contribute to the distortion and thus the flexibility of the cubane structure of the Mn_4CaO_5 cluster, making it easier for the cluster to undergo structural changes during the catalytic cycle (S-state transition). If one assumes that

no H-bonds are present for the oxygen atoms, then not only is the octet rule not met, but also the O-Mn bonds in the cluster become similar to those found in typical Mn oxides, which are in the range of 1.8–2.1 Å. These short distances would yield a rigid, undistorted structure that cannot easily undergo structural changes accompanying the S-state transitions. In other words, the flexibility expected from the distorted structure of the metal cluster would be lost, yielding a compound with little or no catalytic activity for water splitting. It is thus the distorted chair form, or the flexibility, of the Mn_4CaO_5 cluster that is most important for the water-splitting activity. Photosynthetic organisms have gained this extraordinary structure through a long period of evolution and have maintained it for an even longer time, from the advent of prokaryotic cyanobacteria some 2.7 billion years ago to the higher plants that exist today.

The Role of the Ca^{2+} Ion and the Effects of Sr^{2+} Substitution on the Structure of the Mn_4CaO_5 Cluster

Other than Mn, Ca^{2+} is the only metal ion in the Mn_4CaO_5 cluster, and various structural and functional roles have been proposed for it (7, 15, 41, 65, 67, 73, 92, 124, 145). From the structural organization of the Mn_4CaO_5 cluster, it is clear that Ca is needed to maintain the distorted cubane structure owing to its longer bond distances to oxygen atoms compared with those typically found between Mn ions and oxygen atoms. If the cluster were composed only of Mn ions and oxygen atoms, its structure would become symmetric and barely distorted; the resulting compound would be rigid and stable and therefore unable to undergo structural changes. Interestingly, however, QM/MM calculations with the Ca^{2+} ion omitted showed that the distorted structure of the cluster is essentially maintained without that ion (102, 118), suggesting that the role of Ca^{2+} is not solely structural, although small structural changes may occur upon the ion's removal.

The high-resolution PSII structure revealed that two terminal water ligands (W3 and W4) are coordinated to the Ca^{2+} ion (**Figure 2**). W4 is directly H-bonded to Y_Z, and W3 is indirectly H-bonded to Y_Z through another water molecule (52, 127) (**Figure 5**). W3 is also directly or indirectly H-bonded to two water molecules coordinated to Mn4 (W1 and W2), which together with several other water molecules and amino acid residues form extensive H-bond networks around the Mn_4CaO_5 cluster (52, 127) (**Figure 5**). Thus, another important role of the Ca^{2+} ion is apparently to maintain the H-bond network connecting the water molecules and Y_Z (67, 94), some of which must be involved in proton transfer (see below). The H-bonds to Y_Z provided by W3 and W4 must also be important in maintaining the position and orientation of Y_Z (103) in order for it to efficiently mediate electron and proton transfer. This role of the Ca^{2+} ion is apparently fine-tuned and cannot be replaced by a Mn ion, because Ca^{2+} is 7-coordinated and thus able to attract two water molecules, whereas Mn is 6-coordinated (52, 127). The only cation that can replace Ca^{2+} while still partially maintaining the water-splitting activity is Sr^{2+}, which is also 7-coordinated and has the same 2+ charge, with a very slightly larger ionic radius.

The two water molecules bound to the Ca^{2+} ion imply a third, important role for this ion: the binding of one or more substrate water molecules (11, 73, 74, 145). To explore this possibility, Koua et al. (58) replaced the Ca^{2+} ion with Sr^{2+} and used the resulting PSII for crystallization and crystal structural analysis. Because the Sr^{2+}-substituted PSII still exhibited oxygen-evolving activity (at approximately half the level of the Ca^{2+}-containing PSII) (7, 41), the overall structure of the Mn_4CaO_5 cluster is expected to be maintained in the resulting Mn_4SrO_5 cluster. This has been confirmed by EPR, ENDOR (15, 92), and EXAFS measurements. The Sr^{2+} substitution is, however, expected to cause slight structural changes, which may be responsible for the decrease in the oxygen-evolving activity. The crystal structure of the Sr^{2+}-substituted PSII analyzed at a resolution of 2.1 Å showed that the overall structure of the Mn_4SrO_5 cluster was indeed unchanged

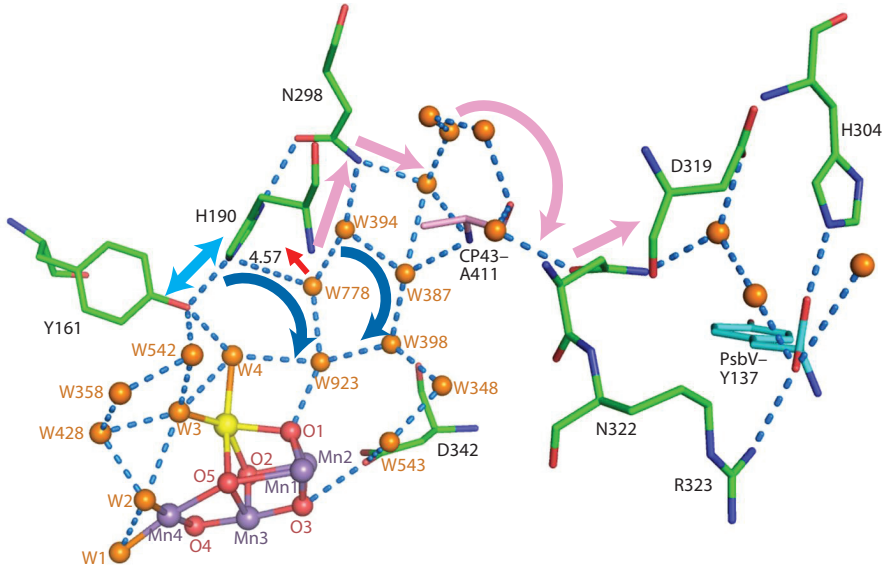

Figure 5

Hydrogen-bond network connecting the Mn_4CaO_5 cluster and Y_Z. The numbering of the water molecules is based on PDB ID 3ARC, with the exceptions of W1–W4. Residues of D1 are in green, a residue of PsbV is in cyan, and a residue of CP43 is in pink. The cyan arrow indicates a possible proton transfer from His190 back to Y_Z, the blue arrows indicate proton paths mediated by several water molecules back to the Mn_4CaO_5 cluster, and the pink arrows indicate proton paths out to the lumenal solution.

compared with that of the Mn_4CaO_5 cluster (58). There were several small differences in the Mn–O and Sr–O distances compared with the corresponding Mn–O and Ca–O distances in the Ca^{2+}-containing PSII, but the most significant difference was in the bond distance between Sr and one of the terminal water ligands (W3), which became 2.6 Å, 0.2 Å longer than the corresponding distance in the Mn_4CaO_5 cluster. By contrast, the W4–Sr distance became 2.3 Å, similar to the corresponding distance (2.4 Å) in the Mn_4CaO_5 cluster. These results suggest that W3 binds to Ca^{2+} more weakly than W4 does and is thus more mobile than W4. In fact, the position of W3 moved by 0.5 Å in the Sr^{2+}-substituted PSII relative to that in the native PSII (58), which also resulted in a breakage of the H-bond between W2 and W3. This implies that W3 may have a higher reactivity than W4, further implying that W3 may be involved in water splitting and O-O bond formation.

HYDROGEN-BOND NETWORKS AND PROTON/WATER CHANNELS

Several possible channels for the exit of protons or entry of substrate water molecules have been proposed based on the cavity space within the protein matrix found in the previous medium-resolution structures (24, 31, 38, 66, 77, 129). For a high-efficiency proton transfer from their production site to the outside of the PSII protein complex, however, H-bond networks are needed through which the Grotthuss mechanism of proton transfer (1) is possible. The high-resolution PSII structure indeed revealed several well-defined H-bond networks leading from the Mn_4CaO_5 cluster to the lumenal bulk solution (52, 127), which may serve as proton exit channels or water inlet channels.

DFT: density functional theory

One of the well-defined H-bond networks involves Y_Z, which mediates electron transfer between the Mn_4CaO_5 cluster and the PSII reaction center Chls. It is well known that upon oxidation by P680, Y_Z donates a proton to D1-His190 and forms a neutral radical, $Y_Z^{\cdot}$ (34, 35, 72, 120). As described above, the crystal structure showed that Y_Z is connected with the oxygen-evolving complex through a well-defined H-bond network (**Figure 5**), and it is further H-bonded with His190 at a distance of 2.5 Å in what has been demonstrated to be a low-barrier H-bond (103, 147). Whether the proton in His190 is released to the outside of the protein complex (the proton-abstraction mechanism) (39, 125) or returns to Y_Z (the proton-rocking mechanism) (12, 96, 97) has been under considerable debate, and the crystal structure has now shown that there are three possible destinations for this proton.

First, the proton may return to Y_Z (the proton-rocking mechanism) (cyan arrow in **Figure 5**), as proposed earlier (12, 96, 97). Second, there is a water molecule, W778 (numbering based on PDB ID 3ARC), 4.6 Å away from His190 (which is H-bonded to Y_Z), and FTIR and density functional theory (DFT) calculations have recently shown that this water molecule moves closer to His190 to make an H-bond with His190 upon oxidation of Y_Z (79). The proton on His190 may come back to the Mn_4CaO_5 cluster first through W778 and then through either W923 or W394-W387-W398-W348-Asp342-W354 (blue arrows in **Figure 5**), as all of these water molecules are ultimately connected to the O1 or O3 atoms in the Mn_4CaO_5 cluster. Third, through the movement of W778, the H-bond network is extended to the lumenal surface by a number of water and amino acid residues (pink arrows in **Figure 5**). This H-bond network is located in the interfaces between the D1, CP43, and PsbV subunits and connected to the lumenal surface through PsbY-Lys129 and PsbV-Tyr137. This H-bond network may function as an exit channel for protons that arise from proton-coupled electron transfer via Y_Z (34, 35, 39, 125). PsbV-Lys129 and PsbV-Tyr137 at the exit of this channel are surrounded by several charged residues, including D1-Arg323 and D1-His304; these residues may therefore function to regulate the proton excretion through the proton-coupled electron-transfer pathway.

Because Y_Z is directly H-bonded to W4 and indirectly connected to W1, W2, and W3, the release of a proton through His190 and the H-bond network enables Y_Z to accept a proton arising from the deprotonation of a substrate water molecule during the S-state transition. Nakamura et al. (79) have suggested that this proton path is functional in the S_2–S_3 transition, although further evidence is required to verify whether and (if so) where this H-bond network works.

Another example of the H-bond network starts from one of the ligands to the Mn_4CaO_5 cluster, D1-Glu333, and is mediated by D1-Asp61 and Cl-1 (52, 127) (**Figure 6**). Cl-1 is one of the two chloride binding sites in PSII, which are located in two sides of the Mn_4CaO_5 cluster and are 6–7 Å away from the Mn_4CaO_5 cluster (51, 78). Cl-1 is surrounded by D1-Lys317, D1-Glu333, and two water molecules (52, 127). The H-bond network extends from D1-Asp61 and Cl-1 through several amino acid residues and water molecules formed by the interfaces of D1, D2, and PsbO, and then to the surface of the protein complex, with several exits in the lumenal bulk solution (**Figure 6**). It may function for the exit of protons or inlet of water molecules (24, 31, 38, 77). In fact, mutagenesis (19) and Cl depletion studies (90, 130) have suggested that both D1-Asp61 and Cl^- ions are important for the activity of oxygen evolution, and several studies have suggested that D1-Asp61 is important for mediating proton transfer.

POSSIBLE MECHANISMS FOR WATER SPLITTING AND O-O BOND FORMATION

Several mechanisms for water splitting and O-O bond formation have been proposed based on the crystal structural analysis; the results of EPR, ENDOR, EXAFS, FTIR, and isotope-exchange

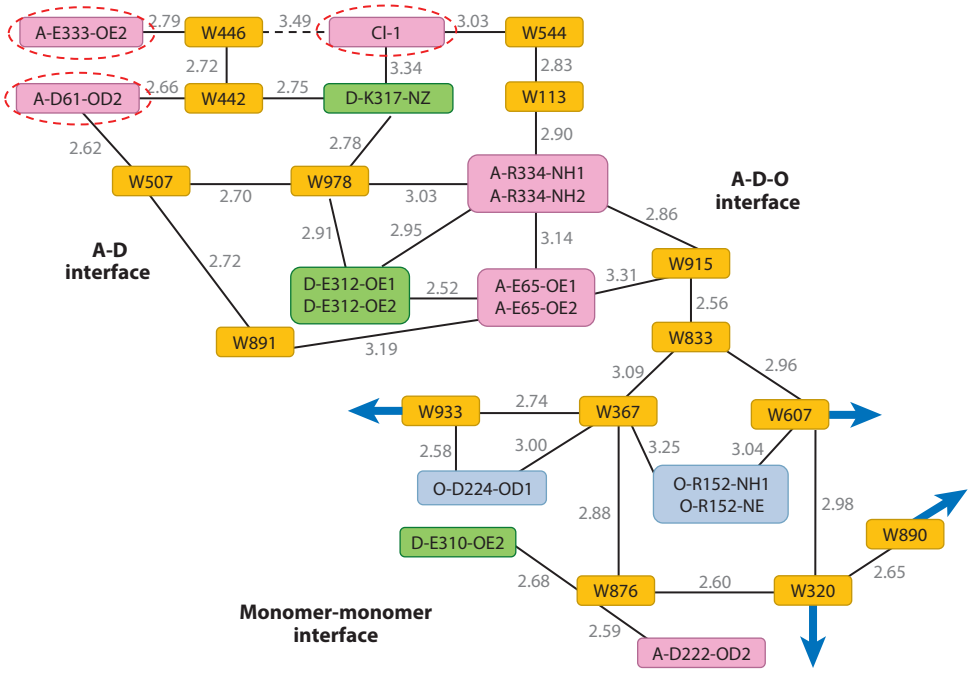

Figure 6

Hydrogen-bond network through Cl-1 and D1-Asp61 (indicated by *red dashed ovals*). The network starts at D1-Glu333 (one of the ligands to the Mn_4CaO_5 cluster, indicated by a *red dashed oval*) and extends through Cl-1, D1-Asp61, and a number of water molecules and amino acid residues provided by D1, D2, and PsbO (33 kDa), with multiple exits (*thick blue arrowheads*) to the lumenal surface. A, D, and O represent PsbA (D1; *pink*), PsbD (D2; *green*), and PsbO (*light blue*), respectively. The distances (in angstroms) are based on the PsbA monomer of the photosystem II dimer in the 1.9-Å structure (PDB ID 3ARC).

experiments; and theoretical calculations (6, 117, 142). The high-resolution crystal structure has provided the possible sites and constraints for water oxidation. Currently, two main types of O-O bond formation can be considered: an oxo-oxyl radical coupling mechanism and a nucleophilic attack mechanism. Each of these mechanisms may involve different sites of the substrates, based on different lines of experimental and theoretical evidence. In the following sections, I discuss the plausible locations of substrates and O-O bond formation in these mechanisms based on the crystal structure as well as other analyses.

O-O Bond Formation Involving the O5 Atom

As discussed above, the O5 atom is unique among the five oxo-bridges in the Mn_4CaO_5 cluster and may participate in O-O bond formation by providing one of the substrate water molecules. The involvement of a bridging oxygen in the O-O bond formation was first proposed by Siegbahn (114, 115) based on extensive DFT calculations, and a recent study using W-band ^{17}O electron-electron double resonance (ELDOR)–detected NMR spectroscopy suggested that the O5 atom could be one of the substrates for O-O bond formation (93, 88). In light of these results, the second oxygen may be provided by an oxyl group deprotonated from a water molecule during the S_2–S_3 or S_3–(S_4) transition or by a terminal water ligand bound to Ca^{2+} or Mn. For the O-O

ELDOR: electron-electron double resonance

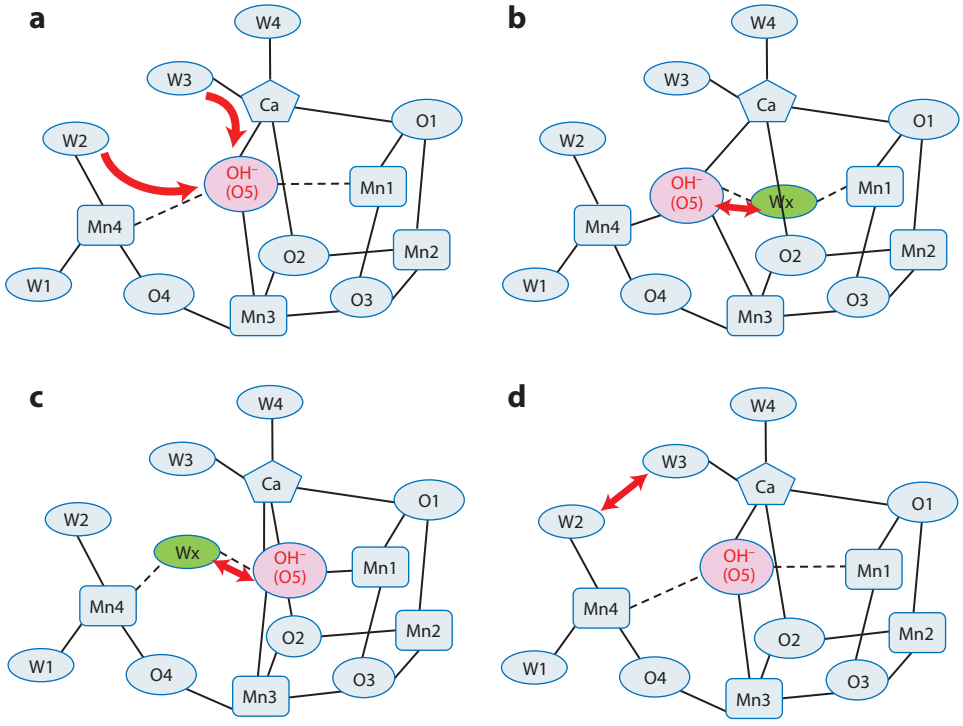

Figure 7

Possible mechanisms for O-O bond formation. (*a*) O-O bond formation between W3 and O5 or between W2 and O5. (*b*) O-O bond formation between O5 and a water molecule (Wx) newly inserted between O5 and Mn1 in the right-side-open (R-type) structure. (*c*) O-O bond formation between O5 and a water molecule (Wx) newly inserted between O5 and Mn4 in the left-side-open (L-type) structure. (*d*) O-O bond formation between W2 and W3 without the involvement of O5.

bond formation involving the O5 atom to be possible, the second substrate water molecule must be close enough to the O5 atom, which may be provided by one of three sites:

1. *O-O bond formation between O5 and W3*: This is a nucleophilic attack mechanism in which the oxo-bridged O5 is attacked by W3, a terminal water ligand to Ca^{2+} (**Figure 7*a***). As described above, substituting Sr^{2+} for Ca^{2+} alters the position of W3 (58), which may be the reason for the decrease of oxygen-evolving activity in the Sr^{2+}-substituted PSII, suggesting that W3 may be directly involved in water splitting. Because W3 is within H-bond distance of O5, it may easily move to become closer to O5 during the S-state transition, leading to O-O bond formation between O5 and W3. This mechanism confers a substrate-binding role on Ca^{2+}, which has also been suggested based on several previous studies addressing Ca^{2+} function (73, 145). This mechanism requires that the two substrate water molecules are already bound in the S_1 state as well as the S_0 state because both W3 and O5 are not likely to be detached in the S_0 state. Time-resolved membrane-inlet mass spectrometry experiments using oxygen-isotope-labeled water detected the binding of two substrate water molecules and showed that at least one of the two substrates is already present in the S_1 state (13, 36, 37) and that two substrate water molecules have already been bound in the S_2 state (81). If one considers that, based on FTIR measurements, no new water molecule is inserted during the S_1–S_2 transition (122), these results suggest that the second water molecule is also bound

in the S_1 state, enabling the formation of the O-O bond between W3 and O5. From the isotope-exchange experiments, however, it is unclear whether the second water molecule is also already present in the S_1 state or comes in at a later step.

2. *O-O bond formation between O5 and W2*: This mechanism is similar to the above, with W2 replacing W3 (**Figure 7*a***). W2 is coordinated to Mn4 and is also within H-bond distance of O5. QM/MM calculations have suggested that W2 is in a deprotonated state in S_1 (2, 64, 93, 99), suggesting that it is a source of proton release during the S-state transition. If this mechanism is indeed in operation, then the two substrate water molecules are coordinated mainly to Mn, and the Ca^{2+} ion does not participate directly in the O-O bond formation, although O5 is also partially connected to the Ca^{2+} ion. As in the O-O bond formation between O5 and W3, this mechanism requires that the two substrate molecules are already bound in the S_1 state.
3. *O-O bond formation between O5 and a newly inserted water molecule*: This is an oxo-oxyl coupling mechanism that was originally proposed by Siegbahn (114, 115) based on the energy cost for O-O bond formation during the final step of S-state transition, and is partially in agreement with the results of recent ELDOR-detected NMR spectroscopic analysis (88, 93). In Siegbahn's original proposal, a new water molecule is inserted between O5 and Mn1 during the S_2–S_3 transition based on the presence of the open space in the dominating R-type structure in the S_2 state (**Figure 7*b***), which then forms an O-O bond with O5 and is released as a dioxygen during the S_3–(S_4)–S_0 transition. This idea is based largely on the fact that in S_2, Mn1 is in a III oxidation state and is 5-coordinated, and there is an open space between Mn1 and O5. Upon one-electron oxidation from S_2 to S_3, Mn1 changes to a IV state and becomes 6-coordinated. The newly inserted water is coordinated to Mn1 to fulfill this requirement. Using DFT calculations, Siegbahn (6, 114–118) showed that the energy barrier for O-O bond formation between O5 and the newly inserted water coordinated to Mn1 is the lowest among all of the possible mechanisms of O-O bond formation. In addition, FTIR measurements have indeed shown the insertion of a water molecule during the S_2–S_3 transition (122). As described above, theoretical calculations have revealed two types of structures in the S_2 state, R-type and L-type structures (**Figure 3**), with the R-type structure dominating in the S_2 state (42, 86). The R-type structure would allow the new water molecule to be inserted between O5 and Mn1, enabling the Siegbahn mechanism to function.

The structural changes that occur during the S_2–S_3 transition, as well as whether the R-type structure is retained and dominates in the S_3 state or immediately before the S_2–S_3 transition, are not clear at present. Recent QM/MM calculations have suggested that the L-type structure is more stable upon transition from S_2 to S_3, and could dominate in the S_3 state (8, 42). In this case, the new water molecule would be inserted (assuming it is indeed inserted) between Mn4 and O5, and therefore the O-O bond formation would occur between O5 and the new water molecule bound to Mn4 (**Figure 7*c***). In either case, according to the crystal structure, the open space between O5 and Mn1 in the R-type structure and between O5 and Mn4 in the L-type structure is rather small, and the O5 atom is protected by a hydrophobic wall provided by a hydrophobic region of a D1 helix between Asn181 and Glu189, within which Val185 is rather close to O5, which may increase the barrier for insertion of the new water molecule. In addition, it is unclear from the FTIR measurements where the new water molecule is inserted during the S_2–S_3 transition and whether it is involved in the current cycle of O-O bond formation or may serve as a substrate for the next cycle of the reaction.

In all of the mechanisms discussed above, the O5 atom must be cut out from its binding site. Although the unusual position of O5 revealed in the crystal structure is consistent with a higher

reactivity of this oxo-bridged oxygen, O5 is connected to four metal ions, and some of the bond distances may become shorter in the higher S states. Indeed, in the R-type or L-type structures obtained for the S_2 state through QM/MM calculations, O5 shifts closer to Mn4 or Mn1, resulting in a stronger binding of O5 to one of these Mn ions (2, 6, 25, 42, 71, 86), as is usually observed in Mn oxides. This makes the cleavage of O5 difficult, creating a higher energy barrier for O-O bond formation involving the O5 atom. Indeed, the cleavage of oxo-bridges to serve as substrates is expected to be more difficult than the cleavage of terminal water ligands, and such cleavage is rarely, if ever, observed in synthetic Mn oxides.

O-O Bond Formation Involving Two Terminal Water Ligands

Because the high-resolution crystal structure revealed four terminal water ligands (W1–W4) to the Mn_4CaO_5 cluster, it is possible that the O-O bond formation could occur within two of these four water ligands via a radical coupling or peroxide-intermediate mechanism without involving an oxo-bridged oxygen. Of these four water molecules, the distance between W2 and W3, two water molecules ligated to Mn4 and Ca^{2+}, respectively, is 3.3 Å (**Figure 2**), and thus they are the most likely candidates for the substrate water molecules. W2 has been suggested to be in a deprotonated state in S_1, indicating that it is one of the proton donors during the S-state transition. W3 may be deprotonated during the S_2–S_3 or S_3–(S_4)–S_0 transition, resulting in two terminally bound OH^- species that may form a peroxide intermediate during the S-state transition, ultimately resulting in the formation of a dioxygen (**Figure 7*d***). This mechanism involves the Ca^{2+} ion and the dangling Mn ion outside of the cubane and requires that the two substrate water molecules are already bound in the S_1 state. The newly inserted water molecules during the S-state transition may be located somewhere outside of the cluster and replace these water molecules after they are deprotonated and released as dioxygen. Therefore, the newly inserted water will be used in the next reaction cycle.

The above mechanism suggests that both Ca^{2+} and a Mn ion (Mn4) are required for water splitting. However, Kusunoki (64) suggested a monomanganese mechanism in which only one Mn ion (the dangling Mn) is involved in water splitting, and the two substrate water molecules are bound to this single Mn ion. Although the crystal structure showed that there are indeed two water molecules, W1 and W2, coordinated to Mn4, and these two water molecules are close enough to form an H-bond, the formation of the O-O bond between them excludes the functional roles of the Ca^{2+} and other Mn ions; thus, this mechanism is less likely.

CONCLUDING REMARKS AND FUTURE PERSPECTIVES

The geometric structure of the Mn_4CaO_5 cluster has been revealed by the structural analysis of PSII at an atomic level, making PSII the largest membrane-protein complex whose structure has been solved at a resolution higher than 2.0 Å. Although there are still some debates regarding the bond distances of Mn–Mn and Mn–O in the crystal structure (possibly owing to radiation damage during X-ray data collection as well as inherent experimental errors), several mechanisms of water oxidation and O-O bond formation could be considered based on the current structure, in which four water molecules were found to be direct ligands to the Mn_4CaO_5 cluster along with a huge number of water molecules in the PSII complex. However, the exact reaction mechanism and possible structural rearrangements occurring during the S-state transitions will become clear only after some (or all) of the structures of the intermediate S states are obtained.

Research in this area will benefit greatly from the high-resolution crystals already obtained as well as a combination of advanced biophysical methods such as X-ray absorption spectroscopy,

advanced EPR techniques, and FTIR. These spectroscopic approaches have yielded unique information regarding the structures, dynamics, and oxidation states of the catalytic site, and in combination with the geometric structure revealed by X-ray crystallography as well as theoretical calculations, they are expected to provide a clear picture of the water-splitting mechanism in the near future. In addition, the availability of X-ray free electron lasers is worth mentioning; these lasers create ultrashort (femtosecond) pulses of intense X-rays that may allow the collection of diffraction data without radiation damage (so-called diffraction before explosion) as well as data collection from short-lived intermediate states (53, 55, 62).

Elucidation of the water-splitting mechanism will be important for the design of an artificial catalyst capable of splitting water using the energy from the sun, an ultimate source of clean and renewable energy. In addition, detailed structural and functional information regarding the roles of protein subunits, amino acid residues involved in water splitting, and proton, water, and oxygen channels in PSII may make genetic modifications possible, which in turn may lead to the enhancement of PSII functions and hence higher plant productivity or better adaptation to adverse environmental conditions.

DISCLOSURE STATEMENT

The author is not aware of any affiliations, memberships, funding, or financial holdings that might be perceived as affecting the objectivity of this review.

ACKNOWLEDGMENTS

I apologize to authors whose work may not have been cited owing to length restrictions. The atomic-resolution structural analysis of PSII described in this article was performed in collaboration with Nobuo Kamiya, Yasufumi Umena, and Keisuke Kawakami, and the analysis of the Sr^{2+}-substituted PSII was performed in collaboration with Faisal H.M. Koua in addition to the above colleagues. I thank these colleagues for their continuous contributions. I also thank Kizashi Yamaguchi for his insightful discussions, Kimiyuki Satoh for reading the manuscript of this review, Chunxi Zhang for discussions, and the past and present members of my laboratory for their contributions in various aspects. The work performed in my laboratory was supported by a Grant-in-Aid for Specially Promoted Research from MEXT/JSPS of Japan (No. 24000018).

LITERATURE CITED

1. Agmon N. 1995. The Grotthuss mechanism. *Chem. Phys. Lett.* 244:456–62
2. Ames W, Pantazis DA, Krewald V, Cox N, Messinger J, et al. 2011. Theoretical evaluation of structural models of the S_2 state in the oxygen evolving complex of photosystem II: protonation states and magnetic interactions. *J. Am. Chem. Soc.* 133:19743–57
3. Barber J. 2004. Engine of life and big bang of evolution: a personal perspective. *Photosynth. Res.* 80:137–55
4. Barber J. 2006. Photosystem II: an enzyme of global significance. *Biochem. Soc. Trans.* 34:619–31
5. Barry BA, Babcock GT. 1987. Tyrosine radicals are involved in the photosynthetic oxygen-evolving system. *PNAS* 84:7099–103
6. Blomberg MR, Borowski T, Himo F, Liao RZ, Siegbahn PE. 2014. Quantum chemical studies of mechanisms for metalloenzymes. *Chem. Rev.* 114:3601–58
7. Boussac A, Rappaport F, Carrier P, Verbavatz JM, Gobin R, et al. 2004. Biosynthetic Ca^{2+}/Sr^{2+} exchange in the photosystem II oxygen-evolving enzyme of *Thermosynechococcus elongatus*. *J. Biol. Chem.* 279:22809–19

8. Bovi D, Narzi D, Guidoni L. 2013. The S_2 state of the oxygen-evolving complex of photosystem II explored by QM/MM dynamics: spin surfaces and metastable states suggest a reaction path towards the S3 state. *Angew. Chem. Int. Ed.* 52:11744–49
9. Bricker TM, Roose JL, Fagerlund RD, Frankel LK, Eaton-Rye JJ. 2012. The extrinsic proteins of Photosystem II. *Biochim. Biophys. Acta* 1817:121–42
10. Britt RD, Campbell KA, Peloquin JM, Gilchrist ML, Aznar CP, et al. 2004. Recent pulsed EPR studies of the Photosystem II oxygen-evolving complex: implications as to water oxidation mechanisms. *Biochim. Biophys. Acta* 1655:158–71
11. Brudvig GW. 2008. Water oxidation chemistry of photosystem II. *Philos. Trans. R. Soc. B* 363:1211–18
12. Christen G, Seeliger A, Renger G. 1999. $P680^{+\cdot}$ reduction kinetics and redox transition probability of the water oxidizing complex as a function of pH and H/D isotope exchange in spinach thylakoids. *Biochemistry* 38:6082–92
13. Cox N, Messinger J. 2013. Reflections on substrate water and dioxygen formation. *Biochim. Biophys. Acta* 1827:1020–30
14. Cox N, Pantazis DA, Neese F, Lubitz W. 2013. Biological water oxidation. *Acc. Chem. Res.* 46:1588–96
15. Cox N, Rapatskiy L, Su JH, Pantazis DA, Sugiura M, et al. 2011. Effect of Ca^{2+}/Sr^{2+} substitution on the electronic structure of the oxygen-evolving complex of photosystem II: a combined multifrequency EPR, ^{55}Mn-ENDOR, and DFT study of the S_2 state. *J. Am. Chem. Soc.* 133:3635–48
16. Dau H, Grundmeier A, Loja P, Haumann M. 2008. On the structure of the manganese complex of photosystem II: extended-range EXAFS data and specific atomic resolution models for four S-states. *Philos. Trans. R. Soc. B* 363:1237–44
17. Dau H, Haumann M. 2008. The manganese complex of photosystem II in its reaction cycle—basic framework and possible realization at the atomic level. *Coord. Chem. Rev.* 252:273–95
18. Dau H, Liebisch P, Haumann M. 2004. The structure of the manganese complex of Photosystem II in its dark-stable S_1-state—EXAFS results in relation to recent crystallographic data. *Phys. Chem. Chem. Phys.* 6:4781–92
19. Debus RJ. 2008. Protein ligation of the photosynthetic oxygen-evolving center. *Coord. Chem. Rev.* 252:244–58
20. Debus RJ, Barry BA, Sithole I, Babcock GT, McIntosh L. 1988. Directed mutagenesis indicates that the donor to P_{680}^{+} in photosystem II is tyrosine-161 of the D1 polypeptide. *Biochemistry* 27:9071–74
21. Diner BA, Rappaport F. 2002. Structure, dynamics, and energetics of the primary photochemistry of photosystem II of oxygenic photosynthesis. *Annu. Rev. Plant. Biol.* 53:551–80
22. Enami I, Okumura A, Nagao R, Suzuki T, Iwai M, Shen JR. 2008. Structures and functions of the extrinsic proteins of photosystem II from different species. *Photosynth. Res.* 98:349–63
23. Ferreira KN, Iverson TM, Maghlaoui K, Barber J, Iwata S. 2004. Architecture of the photosynthetic oxygen-evolving center. *Science* 303:1831–38
24. Gabdulkhakov A, Guskov A, Broser M, Kern J, Müh F, et al. 2009. Probing the accessibility of the Mn4Ca cluster in photosystem II: channels calculation, noble gas derivatization, and cocrystallization with DMSO. *Structure* 17:1223–34
25. Galstyan A, Robertazzi A, Knapp EW. 2012. Oxygen-evolving Mn cluster in photosystem II: the protonation pattern and oxidation state in the high-resolution crystal structure. *J. Am. Chem. Soc.* 134:7442–49
26. Gatt P, Petrie S, Stranger R, Pace RJ. 2012. Rationalizing the 1.9 Å crystal structure of photosystem II—a remarkable Jahn–Teller balancing act induced by a single proton transfer. *Angew. Chem. Int. Ed.* 51:12025–28
27. Gatt P, Stranger R, Pace RJ. 2011. Application of computational chemistry to understanding the structure and mechanism of the Mn catalytic site in photosystem II—a review. *J. Photochem. Photobiol. B* 104:80–93
28. Glöckner C, Kern J, Broser M, Zouni A, Yachandra V, Yano J. 2013. Structural changes of the oxygen-evolving complex in Photosystem II during the catalytic cycle. *J. Biol. Chem.* 288:22607–20
29. Grabolle M, Haumann M, Müller C, Liebisch P, Dau H. 2006. Rapid loss of structural motifs in the manganese complex of oxygenic photosynthesis by X-ray irradiation at 10–300 K. *J. Biol. Chem.* 281:4580–88
30. Grundmeier A, Dau H. 2012. Structural models of the manganese complex of photosystem II and mechanistic implications. *Biochim. Biophys. Acta* 1817:88–105

31. Guskov A, Kern J, Gabdulkhakov A, Broser M, Zouni A, Saenger W. 2009. Cyanobacterial photosystem II at 2.9 Å resolution and role of quinones, lipids, channels and chloride. *Nat. Struct. Mol. Biol.* 16:334–42
32. Haddy A. 2007. EPR spectroscopy of the manganese cluster of photosystem II. *Photosynth. Res.* 92:357–68
33. Haumann M, Müller C, Liebisch P, Iuzzolino L, Dittmer J, et al. 2005. Structural and oxidation state changes of the photosystem II manganese complex in four transitions of the water oxidation cycle ($S_0 \rightarrow S_1$, $S_1 \rightarrow S_2$, $S_2 \rightarrow S_3$, and $S_3{,}_4 \rightarrow S_0$) characterized by X-ray absorption spectroscopy at 20 K and room temperature. *Biochemistry* 44:1894–908
34. Hays AMA, Vassiliev IR, Golbeck JH, Debus RJ. 1998. Role of D1-His190 in proton coupled electron transfer reactions in photosystem II: a chemical complementation study. *Biochemistry* 37:11352–65
35. Hays AMA, Vassiliev IR, Golbeck JH, Debus RJ. 1999. Role of D1-His190 in the proton-coupled oxidation of tyrosine Y_Z in manganese-depleted photosystem II. *Biochemistry* 38:11851–65
36. Hillier W, Wydrzynski T. 2004. Substrate water interactions within the photosystem II oxygen evolving complex. *Phys. Chem. Chem. Phys.* 6:4882–89
37. Hillier W, Wydrzynski T. 2008. ^{18}O-water exchange in photosystem II: substrate binding and intermediates of the water splitting cycle. *Coord. Chem. Rev.* 252:306–17
38. Ho FM, Styring S. 2008. Access channels and methanol binding site to the $CaMn_4$ cluster in Photosystem II based on solvent accessibility simulations, with implications for substrate water access. *Biochim. Biophys. Acta* 1777:140–53
39. Hoganson CW, Babcock GT. 1997. A metalloradical mechanism for the generation of oxygen from water in photosynthesis. *Science* 277:1953–56
40. Ifuku K. 2014. The PsbP and PsbQ family proteins in the photosynthetic machinery of chloroplasts. *Plant Physiol. Biochem.* 81:108–14
41. Ishida N, Sugiura M, Rappaport F, Lai TL, Rutherford AW, Boussac A. 2008. Biosynthetic exchange of bromide for chloride and strontium for calcium in the photosystem II oxygen-evolving enzymes. *J. Biol. Chem.* 283:13330–40
42. Isobe H, Shoji M, Yamanaka S, Umena Y, Kawakami K, et al. 2012. Theoretical illumination of water-inserted structures of the $CaMn_4O_5$ cluster in the S_2 and S_3 states of oxygen-evolving complex of photosystem II: full geometry optimizations by B3LYP hybrid density functional. *Dalton Trans.* 41:13727–40
43. Joliot P. 2003. Period-four oscillations of the flash-induced oxygen formation in photosynthesis. *Photosynth. Res.* 76:65–72
44. Joliot P, Barbieri G, Chabaud R. 1969. Un nouveau modèle des centres photochimiques du système II. *Photochem. Photobiol.* 10:309–31
45. Junge W, Haumann M, Ahlbrink R, Mulkidjanian A, Clausen J. 2002. Electrostatics and proton transfer in photosynthetic water oxidation. *Philos. Trans. R. Soc. B* 357:1407–18
46. Kamiya N, Shen JR. 2003. Crystal structure of oxygen-evolving photosystem II from *Thermosynechococcus vulcanus* at 3.7-Å resolution. *PNAS* 100:98–103
47. Kanady JS, Mendoza-Cortes JL, Tsui EY, Nielsen RJ, Goddard WA, Agapie T. 2013. Oxygen atom transfer and oxidative water incorporation in cuboidal Mn_3MO_n complexes based on synthetic, isotopic labeling, and computational studies. *J. Am. Chem. Soc.* 135:1073–82
48. Kanady JS, Tsui EY, Day MW, Agapie T. 2011. A synthetic model of the Mn_3Ca subsite of the oxygen-evolving complex in photosystem II. *Science* 333:733–36
49. Kanda K, Yamanaka S, Saito T, Umena Y, Kawakami K, et al. 2011. Labile electronic and spin states of the $CaMn_4O_5$ cluster in the PSII system refined to the 1.9 Å X-ray resolution. UB3LYP computational results. *Chem. Phys. Lett.* 506:98–103
50. Kawakami K, Iwai M, Ikeuchi M, Kamiya N, Shen JR. 2007. Location of PsbY in oxygen-evolving photosystem II revealed by mutagenesis and X-ray crystallography. *FEBS Lett.* 581:4983–87
51. Kawakami K, Umena Y, Kamiya N, Shen JR. 2009. Location of chloride and its possible functions in oxygen-evolving photosystem II revealed by X-ray crystallography. *PNAS* 106:8567–72
52. Kawakami K, Umena Y, Kamiya N, Shen JR. 2011. Structure of the catalytic, inorganic core of oxygen-evolving photosystem II at 1.9 Å resolution. *J. Photochem. Photobiol. B* 104:9–18
53. Kern J, Alonso-Mori R, Hellmich J, Tran R, Hattne J, et al. 2012. Room temperature femtosecond X-ray diffraction of photosystem II microcrystals. *PNAS* 109:9721–26

54. Kern J, Loll B, Lüneberg C, DiFiore D, Biesiadka J, et al. 2005. Purification, characterisation and crystallisation of photosystem II from *Thermosynechococcus elongatus* cultivated in a new type of photobioreactor. *Biochim. Biophys. Acta* 1706:147–57
55. Kern J, Tran R, Alonso-Mori R, Koroidov S, Echols N, et al. 2014. Taking snapshots of photosynthetic water oxidation using femtosecond X-ray diffraction and spectroscopy. *Nat. Commun.* 5:4371
56. Kok B, Forbush B, McGloin M. 1970. Cooperation of charges in photosynthetic oxygen evolution. I. A linear four step mechanism. *Photochem. Photobiol.* 11:457–75
57. Kolling DR, Cox N, Ananyev GM, Pace RJ, Dismukes GC. 2012. What are the oxidation states of manganese required to catalyze photosynthetic water oxidation? *Biophys. J.* 103:313–22
58. Koua FH, Umena Y, Kawakami K, Shen JR. 2013. Structure of Sr-substituted photosystem II at 2.1 Å resolution and its implications in the mechanism of water oxidation. *PNAS* 110:3889–94
59. Kuhl H, Kruip J, Seidler A, Krieger-Liszkay A, Bunker M, et al. 2000. Towards structural determination of the water-splitting enzyme. Purification, crystallization, and preliminary crystallographic studies of photosystem II from a thermophilic cyanobacterium. *J. Biol. Chem.* 275:20652–59
60. Kulik LV, Epel B, Lubitz W, Messinger J. 2005. ^{55}Mn pulse ENDOR at 34 GHz of the S_0 and S_2 states of the oxygen-evolving complex in photosystem II. *J. Am. Chem. Soc.* 127:2392–93
61. Kulik LV, Epel B, Lubitz W, Messinger J. 2007. Electronic structure of the Mn_4O_xCa cluster in the S_0 and S_2 states of the oxygen-evolving complex of photosystem II based on pulse ^{55}Mn-ENDOR and EPR spectroscopy. *J. Am. Chem. Soc.* 129:13421–35
62. Kupitz C, Basu S, Grotjohann I, Fromme R, Zatsepin NA, et al. 2014. Serial time-resolved crystallography of photosystem II using a femtosecond X-ray laser. *Nature* 513:261–65
63. Kurashige Y, Chan GKL, Yanai T. 2013. Entangled quantum electronic wavefunctions of the Mn_4CaO_5 cluster in photosystem II. *Nat. Chem.* 5:660–66
64. Kusunoki M. 2011. S_1-state Mn_4Ca complex of Photosystem II exists in equilibrium between the two most-stable isomeric substates: XRD and EXAFS evidence. *J. Photochem. Photobiol. B* 104:100–10
65. Lee CI, Lakshmi KV, Brudvig GW. 2007. Probing the functional role of Ca^{2+} in the oxygen-evolving complex of photosystem II by metal ion inhibition. *Biochemistry* 46:3211–23
66. Linke K, Ho FM. 2014. Water in Photosystem II: structural, functional and mechanistic considerations. *Biochim. Biophys. Acta* 1837:14–32
67. Lohmiller T, Cox N, Su JH, Messinger J, Lubitz W. 2012. The basic properties of the electronic structure of the oxygen-evolving complex of photosystem II are not perturbed by Ca^{2+} removal. *J. Biol. Chem.* 287:24721–33
68. Lohmiller T, Krewald V, Navarro MP, Retegan M, Rapatskiy L, et al. 2014. Structure, ligands and substrate coordination of the oxygen-evolving complex of photosystem II in the S_2 state: a combined EPR and DFT study. *Phys. Chem. Chem. Phys.* 16:11877–92
69. Loll B, Kern J, Saenger W, Zouni A, Biesiadka J. 2005. Towards complete cofactor arrangement in the 3.0 Å resolution structure of photosystem II. *Nature* 438:1040–44
70. Loll B, Kern J, Zouni A, Saenger W, Biesiadka J, Irrgang KD. 2005. The antenna system of photosystem II from *Thermosynechococcus elongatus* at 3.2 Å resolution. *Photosynth. Res.* 86:175–84
71. Luber S, Rivalta I, Umena Y, Kawakami K, Shen JR, et al. 2011. S_1-state model of the O_2-evolving complex of photosystem II. *Biochemistry* 50:6308–11
72. Mamedov F, Sayre RT, Styring S. 1998. Involvement of histidine 190 on the D1 protein in electron/proton transfer reactions on the donor side of photosystem II. *Biochemistry* 37:14245–56
73. McEvoy JP, Brudvig GW. 2006. Water-splitting chemistry of photosystem II. *Chem. Rev.* 106:4455–83
74. McEvoy JP, Gascon JA, Batista VS, Brudvig GW. 2005. The mechanism of photosynthetic water splitting. *Photochem. Photobiol. Sci.* 4:940–49
75. Müh F, Renger T, Zouni A. 2008. Crystal structure of cyanobacterial photosystem II at 3.0 Å resolution: a closer look at the antenna system and the small membrane-intrinsic subunits. *Plant Physiol. Biochem.* 46:238–64
76. Mukherjee S, Stull JA, Yano J, Stamatatos TC, Pringouri K, et al. 2012. Synthetic model of the asymmetric $[Mn_3CaO_4]$ cubane core of the oxygen-evolving complex of photosystem II. *PNAS* 109:2257–62
77. Murray JW, Barber J. 2007. Structural characteristics of channels and pathways in photosystem II including the identification of an oxygen channel. *J. Struct. Biol.* 159:228–37

78. Murray JW, Maghlaoui K, Kargul J, Ishida N, Lai TL, et al. 2008. X-ray crystallography identifies two chloride binding sites in the oxygen evolving centre of Photosystem II. *Energy Environ. Sci.* 1:161–66
79. Nakamura S, Nagao R, Takahashi R, Noguchi T. 2014. Fourier transform infrared detection of a polarizable proton trapped between photooxidized tyrosine Y_Z and a coupled histidine in photosystem II: relevance to the proton transfer mechanism of water oxidation. *Biochemistry* 53:3131–44
80. Nelson DL, Cox MM. 2008. *Lehninger Principles of Biochemistry*. Basingstoke, UK: Palgrave Macmillan. 5th ed.
81. Nilsson H, Rappaport F, Boussac A, Messinger J. 2014. Substrate-water exchange in photosystem II is arrested before dioxygen formation. *Nat. Commun.* 5:4305
82. Noguchi T. 2008. Fourier transform infrared analysis of the photosynthetic oxygen-evolving center. *Coord. Chem. Rev.* 252:336–46
83. Noguchi T. 2008. FTIR detection of water reactions in the oxygen-evolving centre of photosystem II. *Philos. Trans. R. Soc. B* 363:1189–94
84. Noguchi T. 2015. Fourier transform infrared difference and time-resolved infrared detection of the electron and proton transfer dynamics in photosynthetic water oxidation. *Biochim. Biophys. Acta* 1847:35–45
85. Pace RJ, Jin L, Stranger R. 2012. What spectroscopy reveals concerning the Mn oxidation levels in the oxygen evolving complex of photosystem II: X-ray to near infra-red. *Dalton Trans.* 41:11145–60
86. Pantazis DA, Ames W, Cox N, Lubitz W, Neese F. 2012. Two interconvertible structures that explain the spectroscopic properties of the oxygen-evolving complex of photosystem II in the S_2 state. *Angew. Chem. Int. Ed.* 51:9935–40
87. Peloquin JM, Campbell KA, Randall DW, Evanchik MA, Pecoraro VL, et al. 2000. ^{55}Mn ENDOR of the S_2-state multiline EPR signal of photosystem II: implications on the structure of the tetranuclear Mn cluster. *J. Am. Chem. Soc.* 122:10926–42
88. Pérez Navarro M, Ames WM, Nilsson H, Lohmiller T, Pantazis DA, et al. 2013. Ammonia binding to the oxygen-evolving complex of photosystem II identifies the solvent-exchangeable oxygen bridge (μ-oxo) of the manganese tetramer. *PNAS* 110:15561–66
89. Petrie S, Gatt P, Stranger R, Pace RJ. 2012. Modelling the metal atom positions of the Photosystem II water oxidising complex: a density functional theory appraisal of the 1.9 Å resolution crystal structure. *Phys. Chem. Chem. Phys.* 14:11333–43
90. Popelková H, Yocum CF. 2007. Current status of the role of Cl^- ion in the oxygen-evolving complex. *Photosynth. Res.* 93:111–21
91. Pushkar Y, Yano J, Glatzel P, Messinger J, Lewis A, et al. 2007. Structure and orientation of the Mn_4Ca cluster in plant photosystem II membranes studied by polarized range-extended X-ray absorption spectroscopy. *J. Biol. Chem.* 282:7198–208
92. Pushkar Y, Yano J, Sauer K, Boussac A, Yachandra VK. 2008. Structural changes in the Mn_4Ca cluster and the mechanism of photosynthetic water splitting. *PNAS* 105:1879–84
93. Rapatskiy L, Cox N, Savitsky A, Ames WM, Sander J, et al. 2012. Detection of the water-binding sites of the oxygen-evolving complex of Photosystem II using W-band ^{17}O electron-electron double resonance-detected NMR spectroscopy. *J. Am. Chem. Soc.* 134:16619–34
94. Rappaport F, Ishida N, Sugiura M, Boussac A. 2011. Ca^{2+} determines the entropy changes associated with the formation of transition states during water oxidation by Photosystem II. *Energy Environ. Sci.* 4:2520–24
95. Raszewski G, Diner BA, Schlodder E, Renger T. 2008. Spectroscopic properties of reaction center pigments in photosystem II core complexes: revision of the multimer model. *Biophys. J.* 95:105–19
96. Renger G, Kühn P. 2007. Reaction pattern and mechanism of light induced oxidative water splitting in photosynthesis. *Biochim. Biophys. Acta* 1767:458–71
97. Renger G, Renger T. 2008. Photosystem II: the machinery of photosynthetic water splitting. *Photosynth. Res.* 98:53–80
98. Robblee JH, Messinger J, Cinco RM, McFarlane KL, Fernandez C, et al. 2002. The Mn cluster in the S_0 state of the oxygen-evolving complex of photosystem II studied by EXAFS spectroscopy: Are there three di-μ-oxo-bridged Mn_2 moieties in the tetranuclear Mn complex? *J. Am. Chem. Soc.* 124:7459–71

99. Robertazzi A, Galstyan A, Knapp EW. 2011. Can oxidation states and the protonation pattern of oxo-manganese complexes be recognized from their structures? *CrystEngComm* 13:6369–72
100. Robertazzi A, Galstyan A, Knapp EW. 2014. PSII manganese cluster: protonation of W_2, O_5, O_4 and His337 in the S_1 state explored by combined quantum chemical and electrostatic energy computations. *Biochim. Biophys. Acta* 1837:1316–21
101. Roose JL, Wegener KM, Pakrasi HB. 2007. The extrinsic proteins of Photosystem II. *Photosynth. Res.* 92:369–87
102. Saito K, Ishikita H. 2014. Influence of the Ca^{2+} ion on the Mn_4Ca conformation and the H-bond network arrangement in Photosystem II. *Biochim. Biophys. Acta* 1837:159–66
103. Saito K, Shen JR, Ishida T, Ishikita H. 2011. Short hydrogen bond between redox-active tyrosine Y_Z and D1-His190 in the photosystem II crystal structure. *Biochemistry* 50:9836–44
104. Saito T, Yamanaka S, Kanda K, Isobe H, Takano Y, et al. 2012. Possible mechanisms of water splitting reaction based on proton and electron release pathways revealed for $CaMn_4O_5$ cluster of PSII refined to 1.9 Å X-ray resolution. *Int. J. Quantum Chem.* 112:253–76
105. Sauer K, Yano J, Yachandra VK. 2008. X-ray spectroscopy of the photosynthetic oxygen-evolving complex. *Coord. Chem. Rev.* 252:318–35
106. Schinzel S, Schraut J, Arbuznikov AV, Siegbahn PE, Kaupp M. 2010. Density functional calculations of ^{55}Mn, ^{14}N and ^{13}C electron paramagnetic resonance parameters support an energetically feasible model system for the S_2 state of the oxygen-evolving complex of photosystem II. *Chem. Eur. J.* 16:10424–38
107. Shen JR. 2014. Structure-function relationships in the Mn_4CaO_5 water-splitting cluster. In *The Biophysics of Photosynthesis*, ed. J Golbeck, A van der Est, pp. 321–49. New York: Springer
108. Shen JR, Henmi T, Kamiya N. 2008. Structure and function of photosystem II. In *Photosynthetic Protein Complexes: A Structural Approach*, ed. P Fromme, pp. 83–106. Weinheim, Ger.: Wiley-Blackwell
109. Shen JR, Ikeuchi M, Inoue Y. 1992. Stoichiometric association of extrinsic cytochrome c_{550} and 12 kDa protein with a highly purified oxygen-evolving photosystem II core complex from *Synechococcus vulcanus*. *FEBS Lett.* 301:145–49
110. Shen JR, Inoue Y. 1993. Binding and functional properties of two new extrinsic components, cytochrome *c*550 and a 12 kDa protein, in cyanobacterial photosystem II. *Biochemistry* 32:1825–32
111. Shen JR, Kamiya N. 2000. Crystallization and the crystal properties of the oxygen-evolving photosystem II from *Synechococcus vulcanus*. *Biochemistry* 39:14739–44
112. Shen JR, Qian M, Inoue Y, Burnap RL. 1998. Functional characterization of *Synechocystis* sp. PCC 6803 Δ*psb*U and Δ*psb*V mutants reveals important roles of cytochrome *c*-550 in cyanobacterial oxygen evolution. *Biochemistry* 37:1551–58
113. Shoji M, Isobe H, Yamanaka S, Umena Y, Kawakami K, et al. 2013. Theoretical insight into hydrogen-bonding networks and proton wire for the $CaMn_4O_5$ cluster of photosystem II. Elongation of Mn–Mn distances with hydrogen bonds. *Catal. Sci. Technol.* 3:1831–48
114. Siegbahn PE. 2008. A structure-consistent mechanism for dioxygen formation in photosystem II. *Chem. Eur. J.* 14:8290–302
115. Siegbahn PE. 2009. Structures and energetics for O_2 formation in photosystem II. *Acc. Chem. Res.* 42:1871–80
116. Siegbahn PE. 2011. The effect of backbone constraints: the case of water oxidation by the oxygen evolving complex in photosystem II. *ChemPhysChem* 12:3274–80
117. Siegbahn PE. 2013. Water oxidation mechanism in photosystem II, including oxidations, proton release pathways, O–O bond formation and O_2 release. *Biochim. Biophys. Acta* 1827:1003–19
118. Siegbahn PE. 2014. Water oxidation energy diagrams for photosystem II for different protonation states, and the effect of removing calcium. *Phys. Chem. Chem. Phys.* 16:11893–900
119. Styring S, Rutherford AW. 1987. In the oxygen-evolving complex of photosystem II the S_0 state is oxidized to the S_1 state by D^+ (signal II_{slow}). *Biochemistry* 26:2401–5
120. Styring S, Sjöholm J, Mamedov F. 2012. Two tyrosines that changed the world: interfacing the oxidizing power of photochemistry to water splitting in photosystem II. *Biochim. Biophys. Acta* 1817:76–87
121. Sugiura M, Inoue Y. 1999. Highly purified thermo-stable oxygen-evolving photosystem II core complex from the thermophilic cyanobacterium *Synechococcus elongatus* having His-tagged CP43. *Plant Cell Physiol.* 40:1219–31

122. Suzuki H, Sugiura M, Noguchi T. 2008. Monitoring water reactions during the S-state cycle of the photosynthetic water-oxidizing center: detection of the DOD bending vibrations by means of Fourier transform infrared spectroscopy. *Biochemistry* 47:11024–30
123. Suzuki H, Sugiura M, Noguchi T. 2009. Monitoring proton release during photosynthetic water oxidation in photosystem II by means of isotope-edited infrared spectroscopy. *J. Am. Chem. Soc.* 131:7849–57
124. Suzuki H, Taguchi Y, Sugiura M, Boussac A, Noguchi T. 2006. Structural perturbation of the carboxylate ligands to the manganese cluster upon Ca^{2+}/Sr^{2+} exchange in the S-state cycle of photosynthetic oxygen evolution as studied by flash-induced FTIR difference spectroscopy. *Biochemistry* 45:13454–64
125. Tommos C, Babcock GT. 2000. Proton and hydrogen currents in photosynthetic water oxidation. *Biochim. Biophys. Acta* 1458:199–219
126. Tsui EY, Kanady JS, Agapie T. 2013. Synthetic cluster models of biological and heterogeneous manganese catalysts for O_2 evolution. *Inorg. Chem.* 52:13833–48
127. Umena Y, Kawakami K, Shen JR, Kamiya N. 2011. Crystal structure of oxygen-evolving photosystem II at a resolution of 1.9 Å. *Nature* 473:55–60
128. Vass I, Styring S. 1991. pH-dependent charge equilibria between tyrosine-D and the S states in photosystem II. Estimation of relative midpoint redox potentials. *Biochemistry* 30:830–39
129. Vassiliev S, Zaraiskaya T, Bruce D. 2013. Molecular dynamics simulations reveal highly permeable oxygen exit channels shared with water uptake channels in photosystem II. *Biochim. Biophys. Acta* 1827:1148–55
130. Wincencjusz H, van Gorkom HJ, Yocum CF. 1997. The photosynthetic oxygen evolving complex requires chloride for its redox state $S_2 \rightarrow S_3$ and $S_3 \rightarrow S_0$ transitions but not for $S_0 \rightarrow S_1$ or $S_1 \rightarrow S_2$ transitions. *Biochemistry* 36:3663–70
131. Wydrzynski TJ, Satoh K, eds. 2005. *Photosystem II: The Light-Driven Water:Plastoquinone Oxidoreductase.* Dordrecht, Neth.: Springer
132. Yachandra VK, Yano J. 2011. Calcium in the oxygen-evolving complex: structural and mechanistic role determined by X-ray spectroscopy. *J. Photochem. Photobiol. B* 104:51–59
133. Yamaguchi K, Isobe H, Yamanaka S, Saito T, Kanda K, et al. 2013. Full geometry optimizations of the mixed-valence $CaMn_4O_4X(H_2O)_4$ (X = OH or O) cluster in OEC of PS II: degree of symmetry breaking of the labile Mn-X-Mn bond revealed by several hybrid DFT calculations. *Int. J. Quantum Chem.* 113:525–41
134. Yamaguchi K, Yamanaka S, Isobe H, Saito T, Kanda K, et al. 2013. The nature of chemical bonds of the $CaMn_4O_5$ cluster in oxygen evolving complex of photosystem II: Jahn-Teller distortion and its suppression by Ca doping in cubane structures. *Int. J. Quantum Chem.* 113:453–73
135. Yamanaka S, Isobe H, Kanda K, Saito T, Umena Y, et al. 2011. Possible mechanisms for the O-O bond formation in oxygen evolution reaction at the $CaMn_4O_5(H_2O)_4$ cluster of PSII refined to 1.9 Å X-ray resolution. *Chem. Phys. Lett.* 511:138–45
136. Yamanaka S, Kanda K, Saito T, Umena Y, Kawakami K, et al. 2012. Electronic and spin structures of the $CaMn_4O_5(H_2O)_4$ cluster in OEC of PSII refined to 1.9 Å X-ray resolution. *Adv. Quantum Chem.* 64:121–87
137. Yamanaka S, Saito T, Kanda K, Isobe H, Umena Y, et al. 2012. Structure and reactivity of the mixed-valence $CaMn_4O_5(H_2O)_4$ and $CaMn_4O_4(OH)(H_2O)_4$ clusters at oxygen evolution complex of photosystem II. Hybrid DFT (UB3LYP and UBHANDHLYP) calculations. *Int. J. Quantum Chem.* 112:321–43
138. Yano J, Kern J, Irrgang KD, Latimer MJ, Bergmann U, et al. 2005. X-ray damage to the Mn_4Ca complex in single crystals of photosystem II: a case study for metalloprotein crystallography. *PNAS* 102:12047–52
139. Yano J, Kern J, Sauer K, Latimer MJ, Pushkar Y, et al. 2006. Where water is oxidized to dioxygen: structure of the photosynthetic Mn_4Ca cluster. *Science* 314:821–25
140. Yano J, Pushkar Y, Glatzel P, Lewis A, Sauer K, et al. 2005. High-resolution Mn EXAFS of the oxygen-evolving complex in photosystem II: structural implications for the Mn_4Ca cluster. *J. Am. Chem. Soc.* 127:14974–75
141. Yano J, Yachandra VK. 2008. Where water is oxidized to dioxygen: structure of the photosynthetic Mn_4Ca cluster from X-ray spectroscopy. *Inorg. Chem.* 47:1711–26
142. Yano J, Yachandra VK. 2014. Mn_4Ca cluster in photosynthesis: where and how water is oxidized to dioxygen. *Chem. Rev.* 114:4175–205

143. Yeagle GJ, Gilchrist ML, McCarrick RM, Britt RD. 2008. Multifrequency pulsed electron paramagnetic resonance study of the S_2 state of the photosystem II manganese cluster. *Inorg. Chem.* 47:1803–14
144. Yeagle GJ, Gilchrist ML, Walker LM, Debus RJ, Britt RD. 2008. Multifrequency electron spin-echo envelope modulation studies of nitrogen ligation to the manganese cluster of photosystem II. *Philos. Trans. R. Soc. B* 363:1157–66
145. Yocum CF. 2008. The calcium and chloride requirements of the O_2 evolving complex. *Coord. Chem. Rev.* 252:296–305
146. Zein S, Kulik LV, Yano J, Kern J, Pushkar Y, et al. 2008. Focusing the view on nature's water-splitting catalyst. *Philos. Trans. R. Soc. B* 363:1167–77
147. Zhang C. 2007. Low-barrier hydrogen bond plays key role in active photosystem II—a new model for photosynthetic water oxidation. *Biochim. Biophys. Acta* 1767:493–99
148. Zouni A, Jordan R, Schlodder E, Fromme P, Witt HT. 2000. First photosystem II crystals capable of water oxidation. *Biochim. Biophys. Acta* 1457:103–5
149. Zouni A, Witt HT, Kern J, Fromme P, Krauß N, et al. 2001. Crystal structure of photosystem II from *Synechococcus elongatus* at 3.8 Å resolution. *Nature* 409:739–43

Annual Review of Plant Biology

Volume 66, 2015

Contents